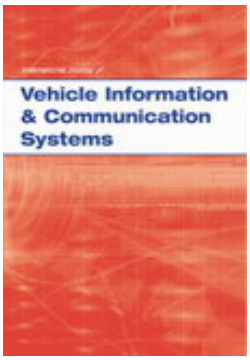

International Journal of Vehicle Information and Communication Systems

ISSN online: 1741-8208 - ISSN print: 1471-0242
https://www.inderscience.com/ijvics

Research on primary traffic congestion point identification method based on fuzzy logic

Haitao Guo, Lunhui Xu

DOI: 10.1504/IJVICS.2023.10057068

Article History:

Received:	26 July 2022
Last revised:	12 December 2022
Accepted:	25 April 2023
Published online:	20 June 2023

Research on primary traffic congestion point identification method based on fuzzy logic

Haitao Guo*

School of Mechanical and Electrical Engineering,
Guangdong Construction Vocational Technology Institute,
Guangzhou, Guangdong, China
and
School of Civil Engineering and Transportation,
South China University of Technology,
Guangzhou, Guangdong, China
Email: guohaitao@gdcvi.edu.cn
*Corresponding author

Lunhui Xu

School of Civil Engineering and Transportation,
South China University of Technology,
Guangzhou, Guangdong, China
Email: xulunhui@scut.edu.cn

Abstract: This study proposes a method to discriminate primary traffic congestion points based on interval type two fuzzy logic combined with improved generative adversarial network, and proposes quantitative congestion point change criteria by using the difference in spatio-temporal order between primary and secondary congestion, and classifies congestion points into four types: primary congestion, primary dissipation, and secondary congestion and secondary dissipation. The methods are also subjected to comparative analysis and ablation experiments to determine the improvement of the optimisation on performance and efficiency. The experimental results show that the method proposed in the study improves the accuracy by 20% to 89% after training, and the average error rate is only 5.5%, which is better than the mainstream congestion point discrimination methods in terms of convergence and efficiency. Finally, the discriminative law of primary traffic congestion points is summarised with the congestion discriminative results of a city for a week.

Keywords: type two fuzzy logic; generative adversarial networks; dual attention mechanism; primary congestion; secondary congestion.

Reference to this paper should be made as follows: Guo, H. and Xu, L. (2023) 'Research on primary traffic congestion point identification method based on fuzzy logic', *Int. J. Vehicle Information and Communication Systems*, Vol. 8, Nos. 1/2, pp.135–151.

Biographical notes: Haitao Guo received his BE in OR from SDU, Shandong, China in 2003. He received his MTech degree in ECE from GDUT, Guangdong, China in 2007. Presently, he is pursuing his PhD degree.

Lunhui Xu is from the Department of Civil Engineering and Transportation, SCUT, Guangdong, China. His areas of interest are traffic control and information engineering, big data and computer vision application.

1 Introduction

The traffic congestion point discrimination system has three main functions, one is the extraction and processing of real-time traffic data, the second is the prediction of traffic flow and the third is the discrimination of congestion point types (Gelman and Kliger, 2020). The prediction of traffic flow is a necessary part of intelligent traffic systems and is important for the design and application of traffic control (Gprf et al., 2020). With the development of computer vision technology and the arrangement of full roadway video surveillance, congestion detection based on video images has become possible (Elyan et al., 2022). In recent years, many scholars have introduced deep learning into the field of traffic congestion discrimination, and the improved AlexNet network proposed by Zhang and Wen (2021) reaches a speed of 0.012s/frame, but it has problems such as bloat and slow speed (Zhang and Wen, 2021). The study sorted out relevant literature, and described traffic congestion, types of traffic congestion and possible economic losses caused by traffic congestion. And briefly introduce the development process of traffic congestion judgment. Referring to some methods of waterway and aviation hub congestion relief and the application of deep learning in traffic congestion judgment, an improved generative adversarial network based on interval type two fuzzy logic is proposed. Its primary traffic jam point identification method is mainly composed of two modules, one is the interval type two fuzzy system responsible for identifying the type of congestion point and the other is an improved generative confrontation network for data processing and traffic prediction. The interval type two fuzzy system is obtained by expanding the type one fuzzy set and setting the affiliation degree fixed to 1. The optimisation of the generative adversarial network is to replace the residual block structure with a dense residual structure and to add a temporal attention mechanism and a spatial attention mechanism in order to improve the prediction performance and efficiency of the neural network.

2 Related work

Traffic congestion refers to the traffic phenomenon in which the traffic flow through a certain section or intersection is larger than the traffic flow due to the increase of traffic demand in a certain period of time, resulting in the detention of some traffic flow on the road. Bhattarai et al. (2019) believed that the main reasons for urban traffic congestion are huge number of cars, low utilisation rate of urban public transportation, residents' disregard for traffic rules and other reasons. According to the causes of traffic congestion, traffic congestion can be divided into frequent congestion and sporadic congestion. According to the influence range of traffic congestion, traffic congestion can be divided into local congestion and network congestion. According to the type of traffic

congestion, traffic congestion can be divided into primary congestion and secondary congestion (Bhattarai et al., 2019). Okuyama et al. (2021) believed that no matter what kind of traffic congestion, it will lead to the increase of social time cost and economic losses and also have a negative impact on the physical and mental health of urban residents. Bista and Paneru (2021) combined qualitative analysis with quantitative analysis to build a multiple regression model. The impact of traffic congestion on urban households and lives was examined through a survey of 160 car owners on six key transport routes in two Nepalese cities. The results of the experiment show that every 2 to 4 km increase in the length of traffic congestion will cause a loss of $25,514 to the car owner (Bista and Paneru, 2021). Therefore, the rapid and accurate identification of traffic congestion has been the focus of domestic scholars. With the development of electronic information technology and detection technology, the recognition of traffic congestion has changed from manual to automatic collection. In the 21st century, scholars at home and abroad have put forward many methods to automatically identify traffic congestion. Yasrebi et al. (2021) proposed a traffic congestion control routing algorithm based on fuzzy logic, which used the uncertainty of fuzzy logic algorithm to enhance the path selection function of network on chip. The results show that the average delay, maximum delay and power consumption of the benchmark algorithm are reduced by 14.88%, 19.39% and 7.98%, respectively (Yasrebi et al., 2021). Tamir et al. (2020) proposed a neural network prediction model based on decision tree and logistic regression to identify traffic congestion. The research results show that the accuracy of decision tree, macro average accuracy and macro average recall rate are 97%, 95% and 96%, respectively, which are much higher than the benchmark model (Tamir et al., 2020). However, in the existing research on traffic congestion identification, it is usually mainly to judge the scale of traffic congestion and the causes of traffic congestion, and there are few studies on the types of traffic congestion. For example, Pei et al. (2021) proposed a method to identify the state and scale of traffic congestion on the main roads of cities in the cold zone based on density clustering, hierarchical clustering and fuzzy C-means clustering, and discussed the characteristics of traffic congestion on the main roads of cities in the cold zone. The results show that this method is suitable for the identification of main road congestion in the cold zone, and can satisfy the spatial autocorrelation and difference test (Pei et al., 2021). Some scholars tend to study how to reduce traffic congestion according to the causes of traffic congestion. For example, Ren (2021) Based on the traffic data of 94 cities in China from 2016 to 2019, built a spatial econometric model, analysed the spatial correlation of public transport enterprise layout and the geographical correlation of urban transport infrastructure and tested the mechanism of their impact on traffic congestion (Ren, 2021). Kasemset et al. (2020) believed that transfer route is an effective measure to avoid traffic congestion, proposed a mathematical model for the location of traffic signs and introduced the application of this method by taking the traffic network of Chiang Mai University as an example. The results show that setting reasonable traffic signs on the road with large traffic flow and high possibility of turning can effectively improve the traffic flow at the gate (Kasemset et al., 2020).

Yan et al. (2019) believed that in the classification of traffic congestion, frequent traffic congestion has certain regularity, which usually occurs at a fixed section or time, while occasional traffic congestion has greater randomness and usually has no regularity. Primary traffic congestion refers to the traffic congestion caused by direct causes, while

secondary traffic congestion refers to the traffic congestion caused by primary traffic congestion (Yan et al., 2019). Qin et al. (2019) believed that as long as the time and place of primary traffic congestion can be immediately identified, the probability of secondary traffic congestion can be reduced and large-scale deterioration of urban traffic flow can be avoided. For the spatio-temporal distribution prediction method of traffic flow, in addition to urban traffic, there are other transport modes can be used for reference. For example, Ma et al. (2021) optimised the timing allocation of coordinated arrival of terminals in order to solve the increasingly serious congestion and delay problems of airports. The optimised modelling takes into account the specific patterns of arriving traffic flow in the terminal area. The experimental results show that the overall delay of the terminal using this optimisation model is reduced by 18.67%, and the delays on the three runways are reduced by 14.56%, 19.35% and 25.37%, respectively (Zhang et al., 2021a). Qi et al. (2021) proposed a spatio-temporal discretisation method based on the concept of standard ships, and established updated rules of ship operation considering the safe distance and collision avoidance time. By simulating the traffic flow of the Yangtze River waterway, it revealed the mechanism of waterway traffic efficiency and safety (Qi et al., 2021). Research using primary congestion and order of space and time relationship between secondary congestion, in this paper, a combined with interval type two fuzzy theory and improve the generated against the assessment method of network congestion point change congestion point can be divided into four types, analysis of the distribution characteristics of various types, in order to rapidly determine the main source of congestion and provide effective reference for policy makers.

3 A generative adversarial network congestion point discrimination method combining interval type two fuzzy theory and improved dual attention mechanism

3.1 Traffic flow prediction module based on interval type two fuzzy theory

A type two fuzzy set is a fuzzy set that extends a type one fuzzy set to give the degree of fuzziness of the affiliation in the set and to improve the ability to describe the fuzziness of the set (Liu and Lin, 2021). Systems built with type two fuzzy sets are type two fuzzy systems and are suitable for dealing with systems whose time-varying characteristics are difficult to construct with mathematical models. The type two fuzzy set theory formula is shown in equation (1).

$$\tilde{A} = \left\{ \left(\left(x, u_A \right), \mu_{\tilde{A}} \left(x, u_A \right) \right) \middle| \forall x \in X, \forall u_A \in J_x \subseteq [0,1] \right\} \tag{1}$$

In equation (1), is a type two fuzzy set defined by $\tilde{A}$ X, A is a type one fuzzy set defined by X, $x \in X$, u_A is a type one fuzzy set affiliation function, and $\mu_{\tilde{A}}$ is a type two fuzzy set affiliation function. The conceptual diagram of type two fuzzy sets is shown in Figure 1.

Figure 1 Concept of type two fuzzy set

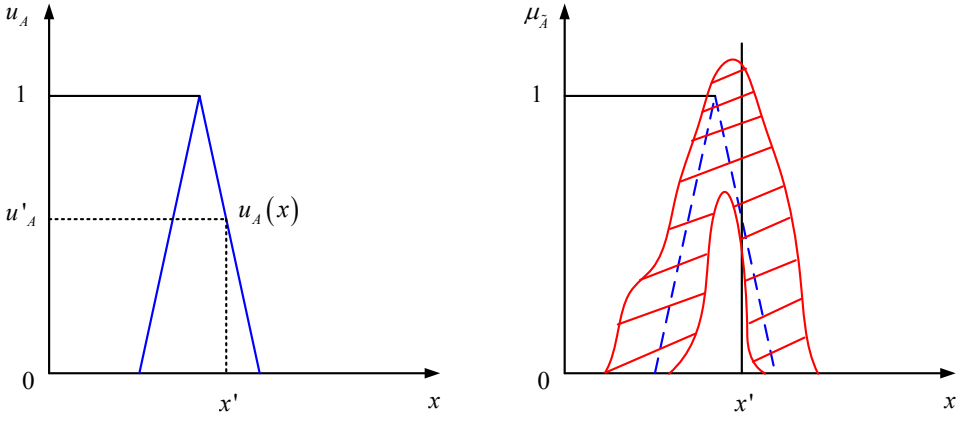

(a)A type of membership function (b)A fuzzy membership function

In Figure 1(a), shifting the function values left and right by unequal distances yields Figure 1(b). For a specific point x' on the *x*-axis, the corresponding function value is no longer a value u'_A, but the range of the line $x = x'$ intersecting the dashed line. Since the corresponding distributions are different, the possibilities of taking the range of values are also different and when $x \in X$ is fuzzified, a type two fuzzy set is obtained. And the standard flow of the row fuzzy system is similar to that of the type one fuzzy system, as shown in Figure 2.

Figure 2 Type two fuzzy system

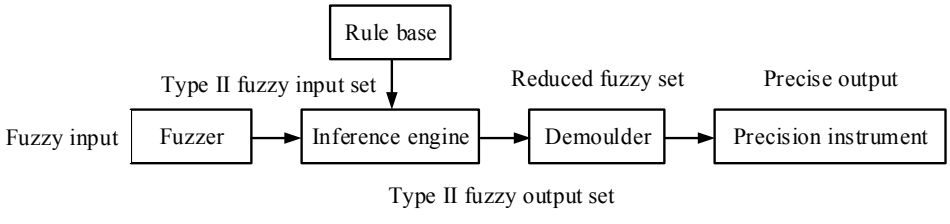

In Figure 2, the input set of type two fuzzy system is obtained by inputting *x* into the fuzzer, and the while line fuzzy output set is obtained by the inference engine under certain rules, and then the reduced fuzzy set is obtained by degeneracy, and finally the exact output is obtained by the exactor. The type reduction operation process of type two fuzzy set is very complicated. When $\forall x \in X, \mu_{\tilde{A}}(x, u_A) = 1$ is satisfied, type two fuzzy set $\tilde{A}$ will become interval type two fuzzy set, as shown in equation (2).

$$\tilde{A} = \int_{x \in X} \int_{u_A \in J_x} 1/(x, u_A)\, du_A dx, J_x \subseteq [0,1] \tag{2}$$

In equation (2), d is the post-fuzzy values. The interval type two fuzzy set has upper-bound affiliation function and lower-bound affiliation function, and the two affiliation

functions intersect to produce the prediction interval of traffic flow, and this study uses Gauss type ground book reading function as the expectation function, as shown in Figure 3.

Figure 3 Membership function of interval type two fuzzy sets

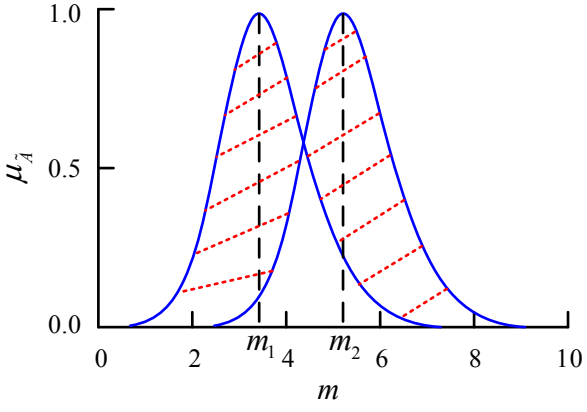

In Figure 3, m is the expected value, and setting the standard deviation σ constant and the expected value m uncertain, equation (3) is obtained.

$$\mu_A(x) = \exp\left[-\frac{1}{2}\left(\frac{x-m}{\sigma}\right)^2\right], m \in [m_1, m_2] \tag{3}$$

In equation (3), each different m, has a corresponding affiliation curve, and the values of m_1 and m_2 depend on the historical data. In the interval type two fuzzy set, the formulas for the upper and lower affiliation functions are shown in equations (4) and (5).

$$\overline{\mu}_{\tilde{A}}(x) = \begin{cases} N(m_1, \sigma; x) & x \le m_1 \\ 1 & , m_1 < x \le m_2 \\ N(m_2, \sigma; x) & x > m_2 \end{cases} \tag{4}$$

$$\underline{\mu}_{\tilde{A}}(x) = \begin{cases} N(m_2, \sigma; x) & x \le (m_1 + m_2)/2 \\ N(m_1, \sigma; x)' & x \ge (m_1 + m_2)/2 \end{cases} \tag{5}$$

When observing the traffic flow in the same area, if the observation time is very short, e.g., 30 minutes, then the traffic flow in the area is random. It will be affected by many factors such as weather, sudden traffic accidents and special traffic flow, but if the observation time is extended to a certain range, then the traffic flow in the area is regular. This study uses the subordination function of type two fuzzy sets to simulate this process in order to achieve the prediction of traffic flow as a basis for determining whether congestion is generated at a certain point. Let the observation time $T_k = [t_{k_1}, t_{k_2}]$, the peak in the range of T_k also seen in the first i day is p_{k_i}, when $m_1 = \min(p_{k_i})$,

$m_2 = \max\left(p_{k_i}\right)$, $\Delta m = \left(m_2 - m_1\right)/n$, the subordination function of m is shown in equation (6).

$$\mu_{m_i} = \mu_m\left(m_i, m_{i+1}\right) = f\left(m_i, m_{i+1}\right)/f\left(m_1, m_2\right) \tag{6}$$

In equation (6), $f\left(m_i, m_{i+1}\right)$ is the frequency of the historical peak $p_k \in \left[m_i, m_{i+1}\right]$. The role of the fuzzy rule is to handle the fuzzy input generated by the affiliation function. Let x_i be the *i*-th component of the input, F_{li} is the *i*-th component of rule l, which corresponds to x_i and y_l be the output function under the *l*-th rule. The fuzzy rules used in this study are shown in equation (7).

$$\begin{aligned} &x_1 = F_{11}, x_2 = F_{22}, ..., x_p = F_{lp} \\ &y_1 = f_1\left(x_1, x_2, ..., x_p\right) \end{aligned} \tag{7}$$

In the fuzzy system, the most critical module is the fuzzy inference module, where the inference engine outputs the affiliation function based on fuzzy input and fuzzy rule calculation, as shown in equation (8).

$$\begin{aligned} &\mu_B\left(y\right) = \prod_{l=1}^{N} \mu_{B_l}\left(y\right) \\ &\mu_{B_l}\left(y\right) = \prod F_{il}\left(x_i\right) \end{aligned} \tag{8}$$

In equation (8), B is the while line output fuzzy set and x_i is the input data. Since the output of the inference engine is a type two fuzzy set, it needs to be degenerated by a degenerator before being exacted by the exactor and the centre-of-mass degenerate method is used in this study, and the obtained centre-of-mass interval is shown in equation (9).

$$y_c\left(x\right) = \frac{\sum_{i=1}^{N} y_i \mu_B\left(y_i\right)}{\sum_{i=1}^{N} \mu_B\left(y_i\right)} \tag{9}$$

The interval is exacted by the exactor to obtain the specific prediction interval. This research adopts fuzzy clustering algorithm to extract fuzzy rules, and the most popular algorithm is fuzzy *c* mean clustering algorithm. However, it has a single object to deal with, and can only deal with point sets, and cannot directly deal with special types of sets such as interval type sets in the face of it. By expanding the sample variance from the point set to the interval set, a new generalised function sample data set is established as the interval data set. Let the sample elements of the data set are in the interval $x_k = \left[x_{k_1}, x_{k_2}\right]$ and the centre of the first i cluster is $\left[p_{i_1}, p_{i_2}\right]$, then the distance of the sample to the cluster prototype is shown in equation (10).

$$d_{ik} = \left(\left\|x_{k_1} - p_{i_1}\right\|^2 + \left\|x_{k_2} - p_{i_2}\right\|^2\right)^{1/2} \tag{10}$$

In equation (10), x_k is the sample and p_i is the cluster prototype. Let U be the set of affiliation functions and P be the set of clustering prototypes, then equation (11) can be obtained.

$$J'_{\omega}(U,P) = \sum_{k=1}^{n}\sum_{i=1}^{c}(u_{ik})^{\omega}(d_{ik})^2 = \sum_{k=1}^{n}\sum_{i=1}^{c}(u_{ik})^{\omega}\left(\left\|x_{k1}-p_{il}\right\|^2 + \left\|x_{k2}-p_{i2}\right\|^2\right) \quad (11)$$

In equation (11), u_{ik} is the affiliation function, ω is the weighting index, $1 \le \omega \le \infty$, c is the number of categories for the clustering algorithm, k is the number of samples and n is the number of samples. Once the data set $X = \left\{\left(x_{k_1}, x_{k_2}\right)\right\}$, the number of clustering categories c and the weighting index ω are determined, the fuzzy classification matrix $\left[u_{ik}\right]$ and the clustering interval centre matrix $\left[p_{i_1}, p_{i_2}\right]$ can be determined.

3.2 Semantic segmentation module combining dual attention mechanism and optimised adversarial generative network

In recent years, convolutional neural networks have been widely used in the field of computer vision, and coupled with the improvement of full roadway video surveillance systems, congestion discrimination based on video images has become possible. Generative adversarial network is a special kind of convolutional neural network, and the standard generative adversarial network cannot utilise all the layered features of the original data, so its underlying structure needs to be optimised (Liu et al., 2021). The optimised underlying structure is shown in Figure 4.

Figure 4 Optimised GAN infrastructure

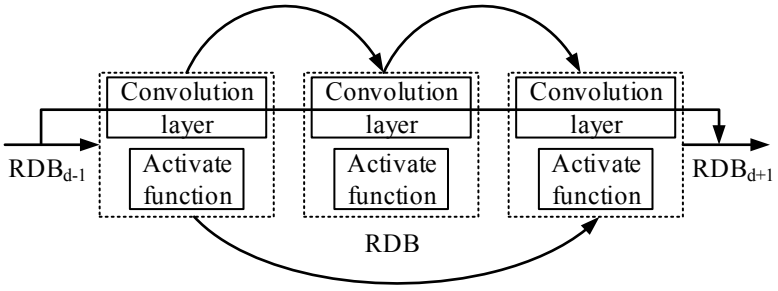

In Figure 4, the Residual Block (RB) structure in the standard GAN is replaced by a dense Residual Block (RDB) structure, which is directly connected between each layer, so it has continuous memory and can fuse the feature information of all layers while fusing the local features of the current layer, which can improve the GAN stability (Zhang et al., 2021b). Let be the input of the F_{d-1} d layer, F_d be the output, and $F_{d,n}$ be the output of the n convolutional layer, the feature output formula is shown in equation (12).

$$F_{d,c} = \delta\left(W_{d,n}\left[F_{d,1}, F_{d,2}, ..., F_{d,n-1}\right]\right) \quad (12)$$

In equation (12), δ is the activation function, $W_{d,n}$ is the weight of the first n convolutional layer and F is the feature mapping. All the feature mappings are concatenated to form the local dense feature, and the compression of the local dense feature is obtained from $F_{d,LF}$ as shown in equation (13).

$$F_{d,LF} = F_d - F_{d-1} \tag{13}$$

Also, because the local features of the image have discontinuities, many edge feature information exists at the connection between the extracted targets and these edge information needs to be detected and extracted. In this study, the gradient detection method is used for edge detection, as shown in equation (14).

$$\nabla f = grad(f) = \begin{bmatrix} g_x \\ g_y \end{bmatrix} = \begin{bmatrix} \dfrac{\partial f}{\partial x} \\ \dfrac{\partial f}{\partial y} \end{bmatrix} \tag{14}$$

In equation (14), ∇ is the *Nabla* operator and ∂ is the step size. The magnitude and direction of the gradient vector are shown in equation (15), and the pixel bias is calculated as shown in equation (16).

$$\begin{aligned} M(x,y) &= M(\nabla f) = \sqrt{g_x{}^2 + g_y{}^2} \\ \alpha(x,y) &= \arctan\begin{bmatrix} g_x \\ g_y \end{bmatrix} \end{aligned} \tag{15}$$

$$\begin{aligned} g_x &= \frac{\partial f(x,y)}{\partial x} = f(x+1,y) - f(x,y) \\ g_y &= \frac{\partial f(x,y)}{\partial y} = f(x,y+1) - f(x,y) \end{aligned} \tag{16}$$

In equation (15), $M(x,y)$ is the magnitude of the gradient vector and α, x, y is the direction of the gradient vector. In equation (16), g_x, g_y is the partial derivative of the pixel. As a kind of discrete differential operator, *Sobel* operator is usually used for edge detection. The object it detects is the discrete pixel in the range of the region. *Sobel* The operator is good at edge processing in both horizontal and vertical directions, and the combination of the for-score derivative and Gaussian smoothing can find the approximate gradient value of the image grayscale function, as shown in equation (17).

$$\begin{aligned} G(i) &= \left| \begin{matrix} \left[f(i+1,j-1) + 2f(i+1,j) + f(i+1,j+1) \right] \\ -\left[f(i-1,j-1) + 2f(i-1,j) + f(i-1,j+1) \right] \end{matrix} \right| \\ G(j) &= \left| \begin{matrix} \left[f(i-1,j+1) + 2f(i,j-1) + f(i+1,j-1) \right] \\ -\left[f(i-1,j+1) + 2f(i,j+1) + f(i+1,j+1) \right] \end{matrix} \right| \end{aligned} \tag{17}$$

In equation (17), G is the gradient of the image $f(x,y)$, and i and j are constants. The process of feature extraction and fusion is shown in Figure 5.

Figure 5 Feature extraction and fusion process

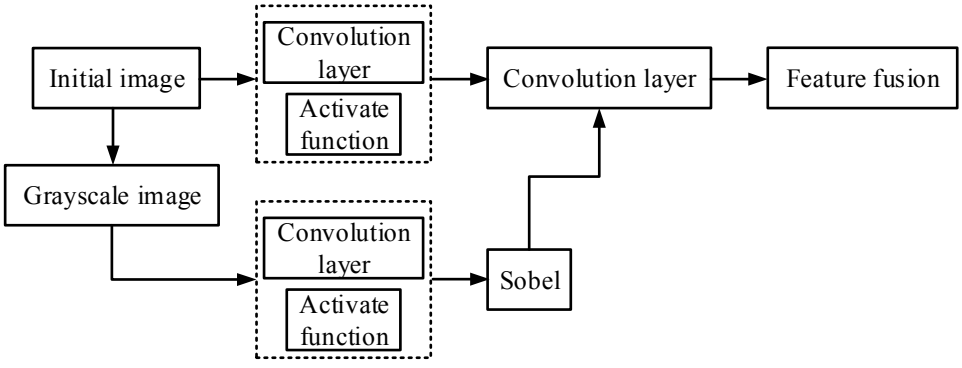

In Figure 5, the input port inputs both the original image and the greyscale image, and the edge feature information in the greyscale image is extracted using the *Sobel* operator edge detection method to maximise the integrity of the image feature information and prevent the accuracy of semantic segmentation from decreasing due to the loss of a large amount of key information. Since traffic flow images have both spatial and temporal dimensions, different attention mechanism modules are added for feature information of different dimensions in order to enhance the detail processing of feature information. The whole semantic segmentation process is shown in Figure 6.

Figure 6 Semantic segmentation process

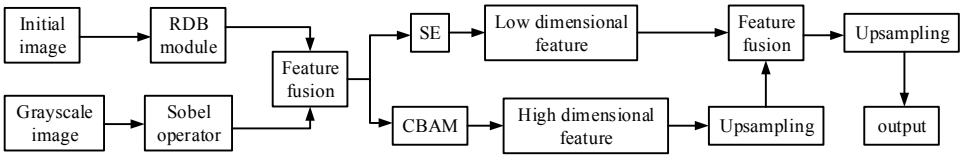

In Figure 6, compared to the standard GAN structure, SE and CBAM modules are added to be able to extract both time-dimensional features and spatial-dimensional features and set high-dimensional features $f^h \in R^{A*H*B}$, which are expanded as shown in equation (18).

$$f^h = \left[f_1^h, ..., f_B^h \right] \left(f_n^h \in R^{A*H} \right) \tag{18}$$

In equation (18), f_B^h is the number of B channels in the high-dimensional feature information, and $f_n^h \in R^{A*H}$ is the n-th high-dimensional feature information in f^h. Each high-dimensional feature information f_n^h has a corresponding feature vector $V^h \in R^B$, which maps V^h to [0, 1] and then normalises the high-dimensional feature information f_{SE}^h with the function *Sigmoid*, as shown in equation (19).

$$f_{SE}^h = F\left(V^h, A\right) = \sigma'\left(fc_2\left(\delta\left(fc_1\left(V^h, A_1\right)\right), A_2\right)\right) \tag{19}$$

In equation (19), σ' is the *Sigmoid* function. The Sigmoid function looks like an *S*-shaped curve and is commonly used to solve binary problems. It has the advantages of smooth curve and easy derivation. A is the fixed parameter in the SE module, δ is the activation function, and fc is the convolution layer. Let the low-dimensional features $f^l \in R^{A*H*B}$, the set of their spatial locations is shown in equation (20).

$$R = \left\{ (x, y) \middle| x = 1, ..., A; y = 1, ..., H \right\} \tag{20}$$

In equation (20), (x, y) is the spatial coordinates of the low-dimensional feature information. V^h is mapped to [0, 1] and then normalised by the *Sigmoid* function to obtain the weighted low-dimensional feature information f_{CBAM}^l, which is expanded as shown in equation (21).

$$\begin{aligned} f_{CBAM}^l &= F\left(f^h, A\right) = \sigma'\left(C_1 + C_2\right) \\ C_1 &= conv_2\left(conv_1\left(f^h, A_1^1\right), A_1^2\right) \\ C_2 &= conv_1\left(conv_2\left(f^h, A_2^1\right), A_2^2\right) \end{aligned} \tag{21}$$

In equation (21), *conv* is the convective layer in the convolutional layer. Given that semantic segmentation is a classification problem, the cross-entropy loss function is used for calculation and the smaller the value of the cross-entropy anytime function, the closer the interval between categories.

4 Experiment and example analysis of each module of traffic congestion point identification method

4.1 Results of method module training and ablation experiments

The method proposed in this study combines an interval type two fuzzy system and a semantic segmentation system with improved adversarial generative networks to be able to discriminate primary traffic congestion points from real-time road condition data. The interval type two fuzzy system uses the HighD data set published by the Institute of Automotive Engineering at RWTH Aachen University, Germany. This data set collects 12-hour measured traffic data from six locations near Cologne, including 5600 complete lane change records. HighD was used as the training set for the type two fuzzy system, and the comparison methods were line graph method and Collaborative Traffic Congestion Check (CoTCC), and the training results are shown in Figure 7.

In Figure 7, the general direction of all three prediction methods is consistent with the actual traffic flow. That is, the traffic volume is in decline in the early morning hours, and starts to rise at 6:00 a.m., reaching the first peak at about 8:00 a.m. The traffic volume remains high from 9:00 a.m. to 16:00 a.m. and then gradually rises to reach the second peak at about 18:00 a.m. The average error rates of the three methods were calculated to be 5.5%, 7.2% and 9.1%. For the training of the semantic segmentation system, 9327 images collected from various neighbourhoods of New York, including street images from different angles and different climates and times of day, are used. The initial learning rate is set to 0.001, the training images used in each iteration are 32, and

the number of iterations is 1000. The ablation experiment method is used to compare the system performance of different modules, as shown in Table 1.

Figure 7 Three prediction methods and practice

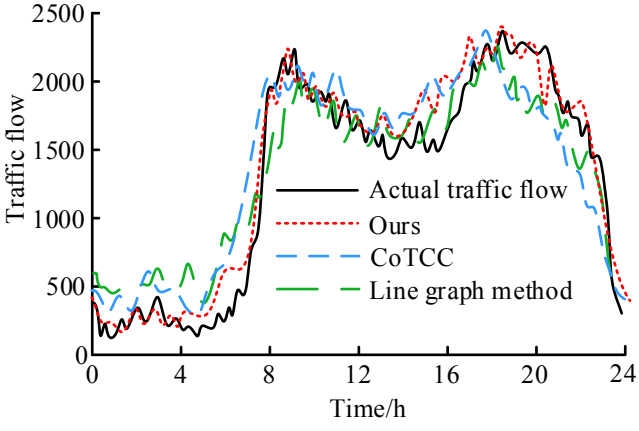

Table 1 Comparison of ablation experiment modules

	Ours	*Verification structure 1*	*Verification structure 2*
RDB	Yes	Yes	No
SE-CBAM	Yes	No	Yes

In Table 1, the validation model 1 only adds the RDB structure without the dual-attention module, and the validation model 2 uses the standard generative adversarial network, adding the dual-attention module. The training results of the three models are shown in Figure 8.

Figure 8 Ablation experiment results

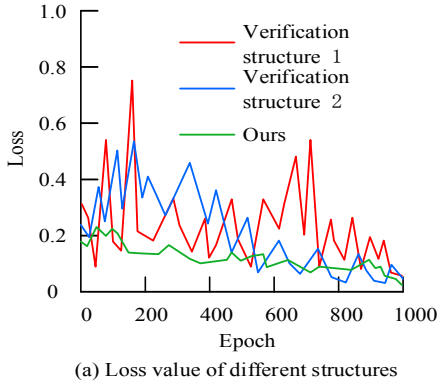

(a) Loss value of different structures

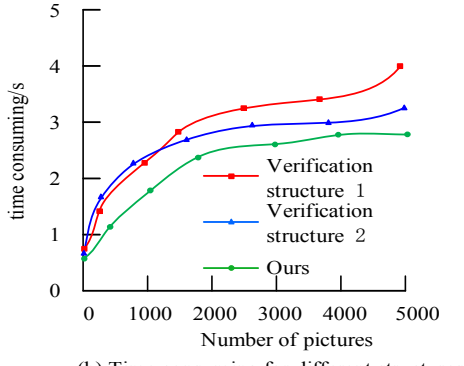

(b) Time consuming for different structures

As can be seen from Figure 8(a), the validation model 1 not only has a high-loss value, but also the loss-value fluctuates a lot, with fluctuation values between 0.2 and 0.4 for every 200 iterations. Although the overall loss value shows a decreasing trend, it still

does not converge after 1000 iterations, and the convergence is poor. The loss value of the validation model 2 fluctuates around 0.2, which is lower than that of the validation model 1. After 500 iterations, the validation model 2 tends to converge and the loss value is lower than 0.1 after convergence, and the fluctuation of the loss value is less than 0.1, which is in accordance with the expectation. From Figure 8(b), it can be seen that as the number of pictures increases, the time consumption of the three models will also increase. Under the same number of pictures, Ours model takes the least time and has the highest efficiency. Combining performance and efficiency as a whole, the optimisation effect of both RDB and SE-CBAM modules on the model is significant. In order to further demonstrate the advantages of the Ours model, four semantic segmentation methods, VGG16, ResNet, Inception and MobileNet, were selected for comparison and the selected data set was Cityscapes. Cityscapes focuses on the semantic understanding of urban streetscapes and is applicable to traffic congestion problems. The comparison of segmentation results is shown in Table 2.

Table 2 Comparison of segmentation accuracy and time consumption

Semantic segmentation method	*Accuracy %*	*Time consuming (5000 pictures)/s*
Ours	97.32	3.1
VGG16	94.58	4.1
ResNet	92.67	4.6
Inception	96.14	4.2
MobileNet	92.09	2.9

In Table 2, the Ours model and the MobileNet model take significantly better time than the other three models, but the MobileNet model has the lowest accuracy rate, 4.23% lower than the Ours model. The Inception model, which has the closest accuracy to Ours, is again much slower than the Ours model, taking 1.5 seconds longer than the Ours model for segmentation of 5000 images. Overall, the Ours model is superior to several mainstream semantic segmentation methods.

4.2 Spatial and temporal discrimination of traffic congestion points based on road forward point differences

The real-time road conditions of a city for a week in December 2020 were used as the validation set to validate the method proposed in this study. The discriminative results of roads with multiple forward direction points are not uniform and can interfere with the analysis results, so these results are combined. Since the inconsistent results account for only about 0.7% of the results, only the type with the highest number of occurrences is recorded in the analysis and only the first type with the same number of occurrences is recorded. The results of discriminating congestion points at different time periods are shown in Figure 9.

Figure 9 Discrimination results of congestion points in different periods

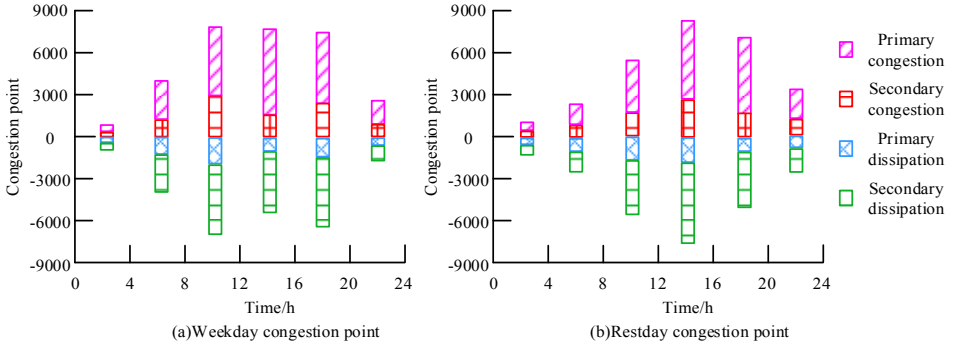

As can be seen from Figure 10, on weekdays, the overall shows two peaks due to the influence of two special hours of the morning and evening peaks, while on rest days, the peaks are not obvious due to the high randomness of travel time and location as people travel mainly for leisure and entertainment, and relatively more people travel in the afternoon. In Figure 9(a), the travel demand increases significantly in the morning and evening peaks on weekdays, and the congestion point is larger than the dissipation point during these two hours, while the dissipation point is larger than the congestion point after the peak period, reflecting the pattern of congestion before dissipation in the process of traffic congestion. The congestion points and dissipation points of other periods and double holidays show a relatively balanced trend. Since primary congestion and secondary congestion have a sequential relationship, secondary congestion points and secondary dissipation points must be located behind primary congestion points and primary dissipation points. On weekdays, the main roads in cities are the most affected areas where primary congestion occurs, especially intersections, which often follow multiple secondary congestion points behind them. In addition to this, there are areas influenced by cultural and commercial values, where the probability of primary congestion is also high. Primary congestion in residential areas is often caused by poor infrastructure or non-compliance with traffic rules. On the other hand, the occurrence of primary congestion points is higher on rest days than on weekdays because people travel relatively regularly on weekdays, while rest days are relatively random and prone to more traffic congestion. Different road points have different spatial locations and have different number of front direction points. Usually, points in road sections have only one front direction point, while road points in and out of side roads usually have two front direction points, intersections will have three front direction points and large interchanges or comprehensive intersections will even have more than three front direction points. In addition, because the roads in this study are not closed roads, there may be extinction of road points with front direction points, the statistics of front direction points of road points in different locations are shown in Table 3.

Table 3 Number of road points in different front directions

	A forward direction points	*Two front direction points*	*Three front direction points*	*Four front direction points*	*No forward direction points*
Road points	7569	341	203	7	69

In Table 3, a total of 8189 road points are selected, and 8120 road points are left after excluding the road points without front direction points. Statistics of the proportion of road points with different front direction points to different types of congestion points are shown in Table 4.

Table 4 Proportion of road points in different front directions to non-passing congestion points

	A forward direction points	*Two front direction points*	*Three front direction points*	*Four front direction points*
The congestion point remains unchanged	92%	91%	91%	71%
Primary congestion point	1%	4%	5%	12%
Primary dissipation point	1%	3%	4%	12%
Secondary congestion point	3%	1%	0%	1%
Secondary dissipation point	3%	1%	0%	1%

In Table 4, the congestion level is constant for most of the roadway points, and the congestion change points are approximately the same at the o'clock where congestion occurs (either primary or secondary). When the road points have only one front direction point, the congestion change points are mainly secondary, while when there are multiple front direction points, the congestion change points are mainly primary. Since the number of road points for one front direction point far exceeds the number of road points for multiple front direction points, it can be concluded that primary road points have a higher probability of appearing in turnoffs (in non-road sections).

5 Conclusion

Distinguishing the spatial and temporal distribution characteristics of primary and secondary congestion is a fundamental prerequisite for solving traffic congestion problems (Autili et al., 2019). The method proposed in the study was experimented and tested and found that the temporal and spatial distributions of primary congestion points are consistent with the daily behavioural characteristics of residents and have a high probability of occurring at traffic intersections of 70 to 90%. Based on this, the proposed method achieves 89% classification accuracy for raw traffic flow data, 97.32% accuracy for traffic congestion point discrimination and 3.1 seconds discrimination time per 5000 images, which is better than the mainstream traffic congestion point discrimination models in both performance and efficiency. The insufficiency of the research lies in ignoring the problem that the continuous congestion point and the continuous congestion road point will continue to spread. The selected comparison model has certain limitations. The improved Xception with Inception structure is not selected, and the dominance of EfficientNet in the imageNet data set is ignored. Future research should introduce a more reasonable comparison model and further improve the model with reference to the squeezed neural network with a lighter structure.

References

Autili, M., Di Salle, A. and Gallo, F. et al. (2019) 'A choreography-based and collaborative road mobility system for L'Aquila city', *Future Internet*, Vol. 11, No. 6. Doi: 10.3390/fi11060132.

Bhattarai, K., Yousef, M., Greife, A. and Lama, S. (2019) 'Decision-aiding transit-tracker methodology for bus scheduling using real time information to ameliorate traffic congestion in the Kathmandu Valley of Nepal', *Journal of Geographic Information System*, Vol. 11, No. 2, pp.239–291.

Bista, R.B. and Paneru, S. (2021) 'Does road traffic congestion increase fuel consumption of households in Kathmandu City?', *Journal of Economic Impact*, Vol. 3, No. 2, pp.67–69.

Elyan, E., Vuttipittayamongkol, P. and Johnston, P. et al. (2022) 'Computer vision and machine learning for medical image analysis: recent advances, challenges, and way forward', *Artificial Intelligence Surgery*, Vol. 2, No. 1, pp.24–45.

Gelman, S. and Kliger, D. (2020) 'The effect of time-induced stress on financial decision making in real markets: the case of traffic congestion', *Journal of Economic Behavior and Organization*, Vol. 185, No. 5, pp.814–841.

Gprf, A., Rim, B. and Jrtn, B. et al. (2020) 'Enhancing intelligence in traffic management systems to aid in vehicle traffic congestion problems in smart cities', *Ad Hoc Networks*, Vol. 107, No. 12, pp.102–117.

Kasemset, C., Boonmee, C. and Arakawa, M. (2020) 'Traffic information sign location problem: optimization and simulation', *Industrial Engineering and Management Systems*, Vol. 19, No. 1, pp.228–241.

Liu, X. and Lin, Y. (2021) 'New efficient algorithms for the centroid of an interval type-2 fuzzy set', *Information Sciences*, Vol. 570, No. 29, pp.468–486.

Liu, Z., Cai, F. and Pan, X. (2021) 'Design and implementation of occlusion image recognition algorithm based on deep convolution generative adversarial network', *Journal of Physics: Conference Series*, Vol. 1883, No. 1, pp.1–7.

Ma, L., Tian, Y. and Yang, S. (2021) 'Collaborative slot allocation for arrival flights in multi-airport terminal area based on the traffic flow pattern: a case study of Shanghai terminal, China', *IOP Conference Series Earth and Environmental Science*, Vol. 638, No. 1, pp.12–17.

Okuyama, R., Mitsume, N., Fujii, H. and Uchida, H. (2021) 'Discontinuous-Galerkin-based analysis of traffic flow model connected with multi-agent traffic model', *Computer Modeling in Engineering and Science*, Vol. 7, No. 9, pp.949–965.

Pei, Y., Cai, X. and Li, J. et al. (2021) 'Method for identifying the traffic congestion situation of the main road in cold-climate cities based on the clustering analysis algorithm', *Sustainability*, Vol. 13, No. 17, pp.1–31.

Qi, L., Ji, Y. and Balling, R. et al. (2021) 'A cellular automaton-based model of ship traffic flow in busy waterways', *Journal of Navigation*, Vol. 74, No. 3, pp.605–618.

Qin, K., Xu, Y. and Kang, C. et al. (2019) 'Modeling spatio-temporal evolution of urban crowd flows', *ISPRS International Journal of Geo-Information*, Vol. 8, No. 12. Doi: 10.3390/ijgi8120570.

Ren, W. (2021) 'The spatial effect of shared mobility on urban traffic congestion: evidence from Chinese cities', *Sustainability*, Vol. 13, No. 24, pp.1–19.

Tamir, T.S., Xiong, G. and Li, Z. et al. (2020) 'Traffic congestion prediction using decision tree, logistic regression and neural networks', *IFAC-PapersOnLine*, Vol. 53, No. 5, pp.512–517.

Yan, X., Liu, X. and Liu, Y. et al. (2019) 'Identification and evaluation of urban traffic congestion based on the big data of floating vehicles and grid modeling', Journal of Beijing Jiaotong University, Vol. 43, No. 1, pp.109–118.

Yasrebi, S., Reza, A., Nikravan, M. and Vazifedan, S. (2021) 'A fuzzy integrated congestion-aware routing algorithm for network on chip', *Frontiers of Information Technology and Electronic Engineering*, Vol. 22, No. 5, pp.741–755.

Zhang, Q., Zhu, Y. and Wang, Z. et al. (2021a) 'Siting and sizing of electric vehicle fast-charging station based on quasi-dynamic traffic flow', *IET Renewable Power Generation*, Vol. 14, No. 19, pp.4204–4214.

Zhang, W. and Wen, J. (2021) 'Research on leaf image identification based on improved AlexNet neural network', *Journal of Physics: Conference Series*, Vol. 2031, No. 1, pp.12–14.

Zhang, Z., Tang, Z. and Wang, Y. et al. (2021b) 'Dense residual network: enhancing global dense feature flow for character recognition', *Neural Networks*, Vol. 139, No. 7, pp.77–85.